# THE SOLAR MASS EJECTION IMAGER (SMEI)

C. J. EYLES[1], G. M. SIMNETT[1], M. P. COOKE[1], B. V. JACKSON[2], A. BUFFINGTON[2], P. P. HICK[2], N. R. WALTHAM[3], J. M. KING[3], P. A. ANDERSON[4] and P. E. HOLLADAY[5]

[1]*School of Physics and Space Research, University of Birmingham, B15 2TT, U.K. (email: gms@star.sr.bham.ac.uk)*

[2]*Center for Astrophysics and Space Science, University of California, San Diego, CA 92093-0424, U.S.A.*

[3]*Space Science Department, Rutherford-Appleton Laboratory, Chilton, OX11 0QX, U.K.*

[4]*Astronomy Department, Center for Space Physics, Boston University, Boston, MA, U.S.A.*

[5]*Air Force Research Laboratory/VSBS, 29, Randolph Road, Hanscom AFB, MA 01731-3010, U.S.A.*

(Received 30 July 2003; accepted 6 August 2003)

**Abstract.** We describe an instrument (SMEI) which has been specifically designed to detect and forecast the arrival of solar mass ejections and other heliospheric structures which are moving towards the Earth. Such events may cause geomagnetic storms, with resulting radiation hazards and disruption to military and commercial communications; damage to Earth-orbiting spacecraft; and also terrestrial effects such as surges in transcontinental power transmission lines. The detectors are sensitive over the optical wave-band, which is measured using CCD cameras. SMEI was launched on 6 January 2003 on the Coriolis spacecraft into a Sun-synchronous polar orbit as part of the US DoD Space Test Programme. The instrument contains three cameras, each with a field of view of $60^\circ \times 3^\circ$, which are mounted onto the spacecraft such that they scan most of the sky every 102-min orbit. The sensitivity is such that changes in sky brightness equivalent to a tenth magnitude star in one square degree of sky may be detected. Each camera takes an image every 4 s. The normal telemetry rate is 128 kbits $s^{-1}$. In order to extract the emission from a typical large coronal mass ejection, stellar images and the signal from the zodiacal dust cloud must be subtracted. This requires accurate relative photometry to 0.1%. One consequence is that images of stars and the zodiacal cloud will be measured to this photometric accuracy once per orbit. This will enable studies of transient zodiacal cloud phenomena, flare stars, supernovae, comets, and other varying point-like objects.

## 1. Introduction

Conventional optical coronagraphs have an optimum response to coronal mass ejections (CMEs) in the plane of the sky. The light detected is photospheric light which has been Thomson-scattered off free electrons within the CME. The response to mass ejections coming towards the observing instrument is relatively poor, except when the ejection is large, and still relatively close to the Sun.

We describe the instrument built by the University of Birmingham and the University of California, San Diego, which has been specially designed to detect CMEs, and in particular those which are heading towards the Earth. Such mass ejections are frequently responsible for geomagnetic storms, which may be ex-

*Solar Physics* **217:** 319–347, 2003.

tremely hazardous to Earth-orbiting spacecraft. Such storms also interfere with satellite communication and surveillance systems, and cause disruption to transcontinental power lines. The radiation enhancements which accompany the CMEs/geomagnetic storms are potentially hazardous to astronauts.

The Solar Mass Ejection Imager (SMEI) is currently flying on the US Department of Defence Space Test Program 'Coriolis' mission. It was launched on 6 January 2003 from Vandenberg Air Force Base in California. Coriolis was inserted into an 840-km circular, Sun-synchronous polar orbit along the Earth's terminator. The philosophy behind the SMEI concept, and some of the historical perspective, may be found in Jackson *et al.* (2003).

## 2. The Instrument Requirements

The data from photometers on the HELIOS spacecraft (Leinert *et al.*, 1981) demonstrated that it was possible to detect solar mass ejections (Jackson and Leinert, 1985). Jackson and Hick (2002) have applied tomographic techniques to the HELIOS data to map various density features in the inner heliosphere. The signal from Thomson scattering is very faint, and this places stringent requirements on the performance of the instrument. Figure 1 shows the brightness of various features within the heliosphere as a function of solar elongation. The intensity scale is measured in terms of the equivalent brightness of a $10^{th}$ magnitude star in a square degree (one S10 unit). The background starlight is close to the zodiacal light at elongations $> 90°$. However, a typical large CME is well below this level. Thus in order to extract the signal from CMEs and other transients of similar brightness, the instrument must be capable of accurate photometry and have a dynamic range of at least four orders of magnitude. We have therefore chosen the CCD camera to have a 16-bit analogue-to-digital converter, which gives an instrument dynamic range in the region of 50 000. The tomographic analysis requires 0.1% photometry and background light reduction below the one-S10 level. This translates to a $10^{-15}$ surface brightness reduction relative to the solar disc. SMEI achieves this reduction in stray light through the design of the baffle ($10^{-10}$) and the optics chamber ($10^{-5}$) (Buffington, Jackson, and Hick, 2002).

The telemetry allocation to SMEI for normal operations is 128 kbits $s^{-1}$. The basic angular resolution of the camera is 0.05° pixel$^{-1}$; however under normal operations this is degraded to 0.2° by $4 \times 4$ on-board binning ($2 \times 2$ for the camera viewing nearest the Sun). We then transmit a region of interest on the CCD chip covering the sky image for each camera every 4 s. Fitting these data into the allocated telemetry is achieved in the on-board data system via a Rice compression algorithm.

Other requirements on the system are that the imaging response should be extremely uniform, otherwise both pixel-to-pixel variations and sub-pixel gradients in the CCD would make the required stellar subtraction difficult (Buffington, Hudson,

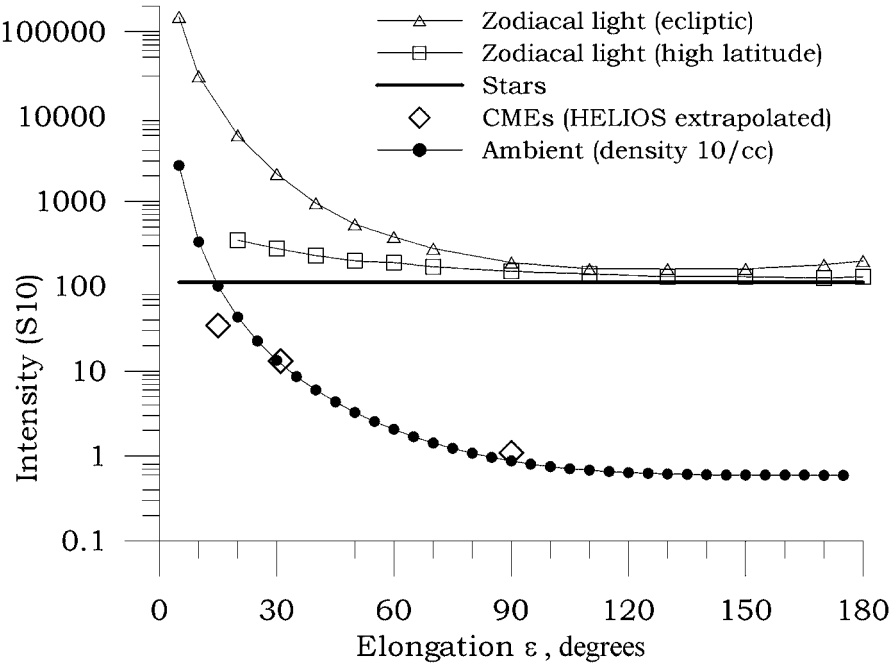


*Figure 1.* Sky surface brightness versus solar elongation, $\epsilon$, for zodiacal light and starlight; and the expected brightness of one of the larger CMEs extrapolated from the photometer on the HELIOS spacecraft. The lowest line (*black filled circles*) shows the calculated brightness of an ambient medium with a mean density of 10 electrons $cm^{-3}$ at 1 AU. The intensity scale is in S10 units, which is the equivalent brightness of a $10^{th}$ magnitude star in a square degree. (After Buffington, Jackson, and Hick, 2002.)

and Booth, 1990; Buffington, Booth, and Hudson, 1991). There is a jitter requirement on the spacecraft, which translates into a maximum of 0.15° peak-to-peak in 4 s at the $3\sigma$ level.

The mass of SMEI is 36 kg and the power consumption during normal operation is approximately 22 W.

## 3. The Instrument Architecture

SMEI consists of three identical sensors mounted at different viewing angles to the Sun on the Coriolis spacecraft. The detection technique is via a CCD operating in the optical part of the spectrum. The actual bandpass is from 450–950 nm, which is the response window of the CCD for a quantum efficiency of $> 10\%$. The main optics chamber, which contains the CCD chip, is also the prime structural element which interfaces to the spacecraft. To this chamber are attached the baffle system and the CCD camera electronics. The CCD is an E2V Technologies (formerly EEV Ltd) CCD05-30-231A frame transfer device, which has an image area of

*Figure 2.* One of the three SMEI camera units, shown mounted to an interface plate which was used in vibration qualification.

1242 × 576 pixels (22.5 $\mu$m). The CCD is cooled via a passive radiator which is coupled to the CCD via a thermally-isolated cold finger. The radiators for each camera are oriented so that when mounted on the spacecraft, each views deep space as much as possible.

The instrument is controlled by a data handling unit (DHU) which contains a dual redundant microprocessor system, based on a Texas Instruments SMJ320C50AHFGM-40 digital signal processor running at 19 MHz. Each half of the DHU interfaces with the spacecraft via a MIL-STD-1553B bus. The on-board software is stored (eight copies) in $E^2$PROM; this software is designed to accommodate software updates should they be necessary.

Figure 2 is a photograph of one of the flight model camera units, mounted on an interface plate which was used in vibration qualification. On the left is the

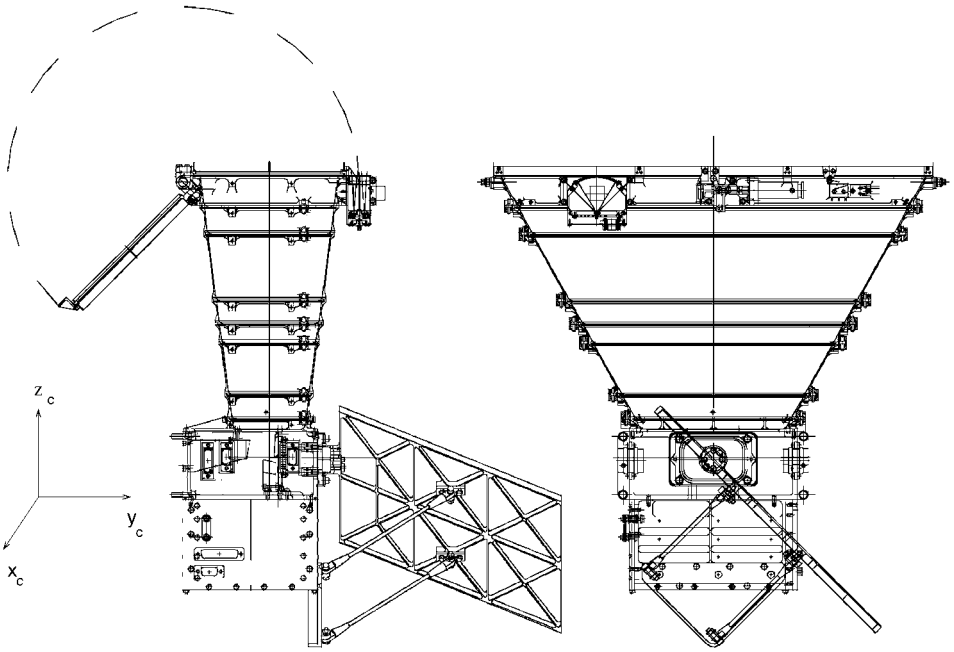


*Figure 3.* Two cross-sections of one of the camera units (see text).

door covering the entrance to the baffle. The door hinge is on the bottom, and the latch mechanism is mounted on the top of the baffle. Also mounted on the top of the baffle is the bright object sensor, which senses if the Sun comes within approximately 7° of the edge of the field of view and closes the shutter. In the centre of the camera unit is the optics chamber, which contains the mirrors used to form the image and the CCD chip. The cold finger comes out through the top of this chamber, where it is connected to the passive radiator. The CCD electronics chamber is mounted to the optics chamber on the right side, and the supports for the radiator are attached to one edge of the electronics box.

The field of view of each camera is approximately rectangular, covering a fan-beam area of the sky $60° \times 3°$. Figure 3 shows cross sections of a camera unit across the 3° and 60° directions, respectively. In the section on the left, the tapered baffle is shown attached to the central rectangular optics chamber, which interfaces to the spacecraft on the left side. Below that is the CCD camera electronics box, which has a bracket to support the passive radiator for the CCD. This radiator is attached to the cold finger which goes through the right face of the optics chamber. At the inner end of the cold finger is the CCD chip itself.

At the top (front) of the baffle is the door, which is shown in the open position; the dashed arc indicates the envelope it requires in order to open. The protrusion at the right is the bright object sensor and the latch mechanism. Both of these are seen better in the right section, which covers the 60° side of the field of view. The

bright object sensor is at the top left, while the door latch mechanism is near the top centre. The latch is released via the operation of a High Output Paraffin (HOP) actuator, which is the cylindrical structure extending to the right. The baffle is made in nine sections, eight of which may be seen in both views.

We now describe the various subsystems which make up the whole instrument.

### 3.1. THE OPTICAL DESIGN

The optical design is in two parts. The first is the design of the baffle and the second is the imaging section.

#### 3.1.1. *The Baffle*

The design and laboratory measurements of the SMEI baffles are described in detail by Buffington, Jackson, and Hick (2002). A labyrinthine baffle controls stray light by combining a hierarchical sequence of aperture openings, each positioned to block a view of its previous neighbor, with blackened surfaces that absorb rather than scatter most of the unwanted light. Briefly, the design exploits SMEI's asymmetrical field of view to provide three baffle stages in one projection, and two stages in the other. Figure 4 illustrates the baffle's arrangement of apertures and connecting septums. In Figure 4(a) the three stages are defined respectively by apertures Z0 to Z3, Z3–Z6, and finally Z6–Z8. Secondary apertures placed between these further improve performance by reducing single-scattering paths through each stage (Buffington, Jackson, and Hick, 2002). Some of these secondary apertures (Z4 and Z5) are effective only in the narrow dimension, while Z1 and Z7 only partially cover their respective bottom primary aperture faces. Vane opening Z0 defines the SMEI entrance pupil. A cross-section of the baffle in the wide dimension is shown in Figure 4(b).

A critical element in the design, if the SMEI specification is to be met, is to achieve a sufficiently low reflectivity that four scatters plus the aperture geometry reduces the stray light below $10^{-10}$. The internal surfaces of the baffle sections were treated with an optically-absorbent coating known as Martin Black (Martin Marietta Company, 1977) which has a nominal reflectivity across the optical band of 0.005. Measurements on the SMEI flight baffles confirmed this (Buffington, Jackson, and Hick, 2002) and also demonstrate the expected $10^{-10}$ light reduction through Z0 relative to direct sunlight.

The remaining important design consideration is the treatment of the aperture edges. When aperture edges Z6, Z5, or Z4 are directly illuminated some light scatters off the edge, which may go towards Z0 or close to the edge of Z3. Also, diffraction of only a few degrees at one of the later baffle edges for light originating at the primary baffle edge Z6 can cause it to enter the aperture Z0. To reduce the effect of the edges they were machined with a 30° bevel tapering down to a blunt edge of $0.25 \pm 0.05$ mm in width. When the Martin Black surface treatment is applied, the edge is rounded to a cylindrical shape of radius approximately 0.2 mm. The

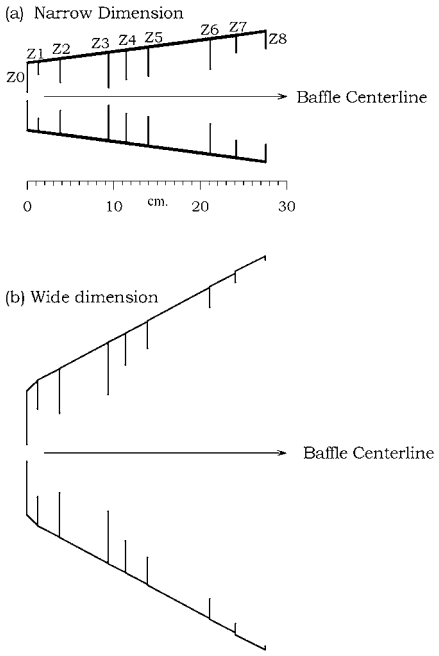


*Figure 4.* (a) A cross-section of the baffles across the narrow dimension. The entrance pupil is Z8 and the exit pupil Z0. (b) A cross-section of the baffles across the wide dimension.

complete analysis of the performance of the SMEI baffle is given by Buffington, Jackson, and Hick (2002), who show that it should meet the SMEI specification.

### 3.1.2. *The Imaging System*

The second element in the SMEI optical design is the imaging system, which is located beyond the instrument pupil, aperture Z0 in Figure 4. The SMEI optics use two mirrors to focus the sky onto the CCD. The resulting illumination lies within a circular arc on the CCD which is about 100 pixels wide and subtends just over 60° on the sky. This then covers essentially the full 1242-pixel available width of the CCD.

The five important elements in this part of the system are shown in Figure 5. Light enters through aperture Z0 and is then focused by the primary mirror M1 towards conical mirror M2. This mirror serves to flatten the image onto the planar CCD surface. The fourth element is a vane (V) which performs some of the function of a Lyot stop. This intercepts unwanted light that reflected from M1 but originated outside of the field of view. This includes sky objects beyond the field of view, but also stray light which finds its way through the baffle. This latter light mostly scattered last from the edge or rear of aperture Z3 (Buffington, Jackson, and Hick, 2002), but may also be stray light scattering inside the optics enclosure which entered through Z0 at a large angle. The fifth optical element is the CCD itself.

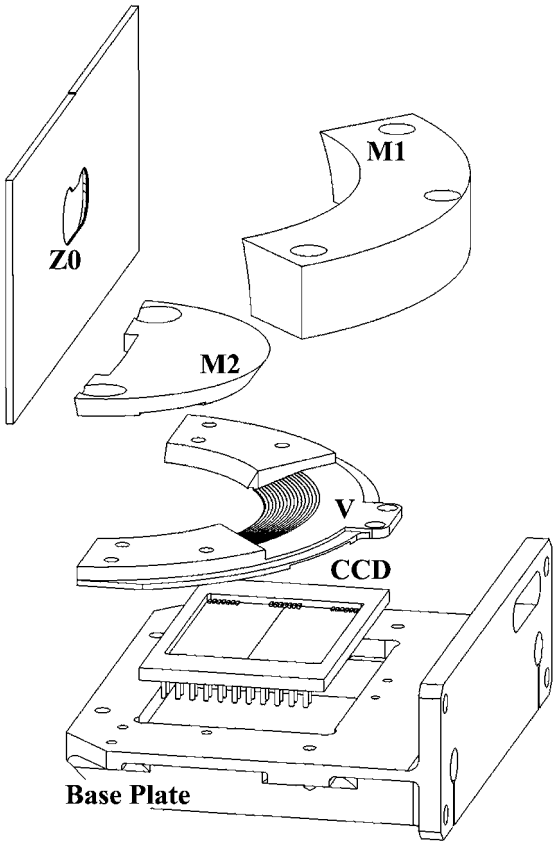


*Figure 5.* Exploded view of the SMEI optics. See also Figures 6 and 7. Light enters the optics chamber from the left through the final aperture Z0 of the baffle. It then reflects from mirrors M1 and M2 and travels downwards to the CCD. Vane V serves some of the function of a coronagraphic Lyot stop by blocking light from outside of the field of view (Figure 7). The series of steps (0.1 mm increments in height) shown on its gradual sloped portion nearest the CCD are required to remove background light which reached the CCD by grazing-angle reflection from V when this surface was made smooth. The imaging portion of the CCD is the left-hand rectangle in this view, whereas the covered (frame-store) portion is the right-hand rectangle. These optical components, except the aperture and CCD, are all mounted to the base plate shown, and this portion of the optics is entirely enclosed by the main mechanical structure and provided with a shutter controlled by the on-board processor (DHU) immediately behind Z0 and just above M2.

Figure 6 shows the optics layout with the light path incident at 0° highlighted. Figure 7 shows a cross-section through the optics mid plane with rays traced at $\pm 2.5°$. This figure illustrates the function of vane V, which in each extreme case intercepts a portion of the light. It is clear from Figure 6 that the CCD is close to M2; the design separation between the (windowless) CCD surface and the bottom of mirror M2 is only 1.0 mm, a serious concern for the thermal and mechanical

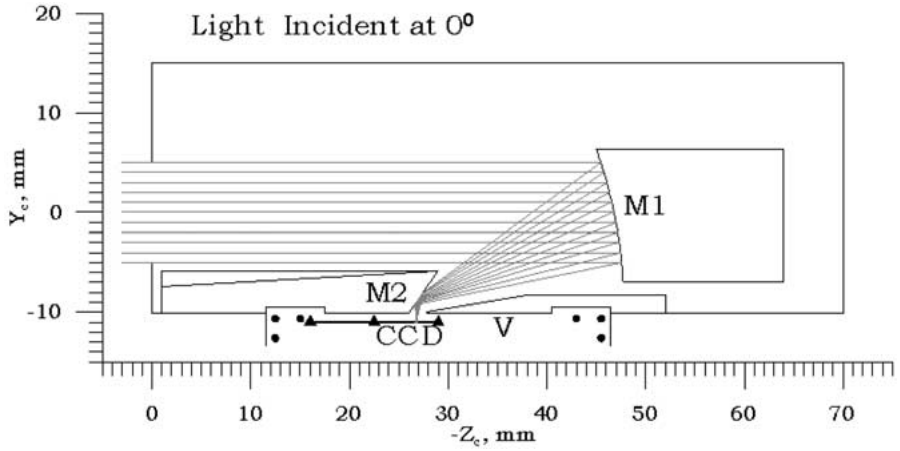


*Figure 6.* A cross-section through the optical system showing normally incident light entering through the exit pupil of the baffle ($Z = 0$), reflecting from mirrors M1 and M2 and reaching the CCD. The imaging portion of the CCD is indicated by the solid filled triangles, while the frame-store part is beneath vane V.

design, see discussion below. The three solid dots indicate the position of the corners of the ceramic frame holding the CCD chip itself.

A key SMEI specification is 0.1% differential photometry. This follows directly from the SMEI prime objective, observation of coronal mass ejections, which requires an effective subtraction of the stellar background and zodiacal light down to below 1 S10 unit. Briefly, the SMEI optics design is a Newtonian reflector in one projected plane, and a Schmidt camera without its corrector plate in the other. The optical system is a very fast design, namely $f/1.2 \times f/2.2$. Unresolved images in very fast optical systems usually suffer from 'hot spots' that would compromise 0.1% photometry through pixel-to-pixel response variations, and sub-pixel response gradients (Buffington, Hudson, and Booth, 1990; Buffington, Booth, and Hudson, 1991). However, this particular design exploits a fortunate compromise in which the light converges prior to reaching the CCD in the 'Newtonian' projection, and after it in the other. The resulting unresolved stellar image shape is shown in Figure 8. Although a hot spot does exist at the centre of this image, sufficiently little of the light is concentrated there to preclude the 0.1% photometry. The design yields image shapes that change little along the long dimension of the field of view.

Mirror M1 was made from a diamond-turned aluminum ring, of the correct figure, which was then separated into quadrants of the correct size. The quadrants were separated prior to the final machining to avoid possible figure change due to stress relief upon separation. M2 was made similarly, but in semicircular segments. The resulting mirrors have a surface waviness of period one to several millimetres, and the amplitude must be kept sufficiently small so as not to contribute significantly to image size growth. To meet the SMEI specification the maximum amplitude that could be tolerated was around 3 $\mu$m peak-to-peak.

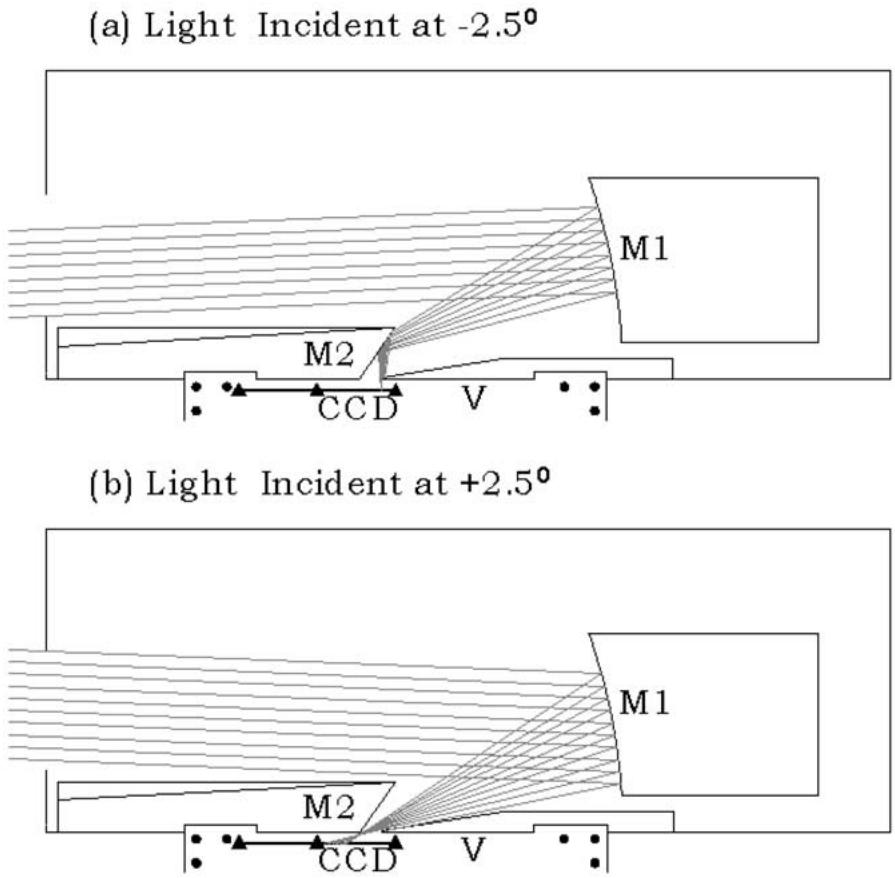


*Figure 7.* A cross-sectional view as in Figure 6, but with the axes suppressed, and with light entering at $-2.5°$ (a) and $+2.5°$ (b). In (a) rays reflecting from M1 but hitting the top of M2 are not shown. In (b) the lowest ray, also not shown, intercepts the top of M2 before reaching M1. In both cases illustrated vane V intercepts a portion of the light.

The remaining factors in the optical design are the alignment tolerance of the main components and the surface finish of the chamber within which they are mounted. The optics chamber has to provide the additional $10^{-5}$ stray-light rejection to meet the total SMEI specification. This was achieved through careful design of the mirror mounts for M1 and M2, the design of vane V, and a black anodized interior surface finish.

The most demanding alignment parameter relates to the position of M2 with respect to the CCD. This is particularly awkward because in flight the CCD chip is at around $-30$ °C, while during integration and testing the temperature is around 20 °C. Figure 6 shows that M2 is sandwiched closely between the CCD and the volume occupied by the incident light. The clearance between the CCD and M2 is slightly less than 1 mm at room temperature.

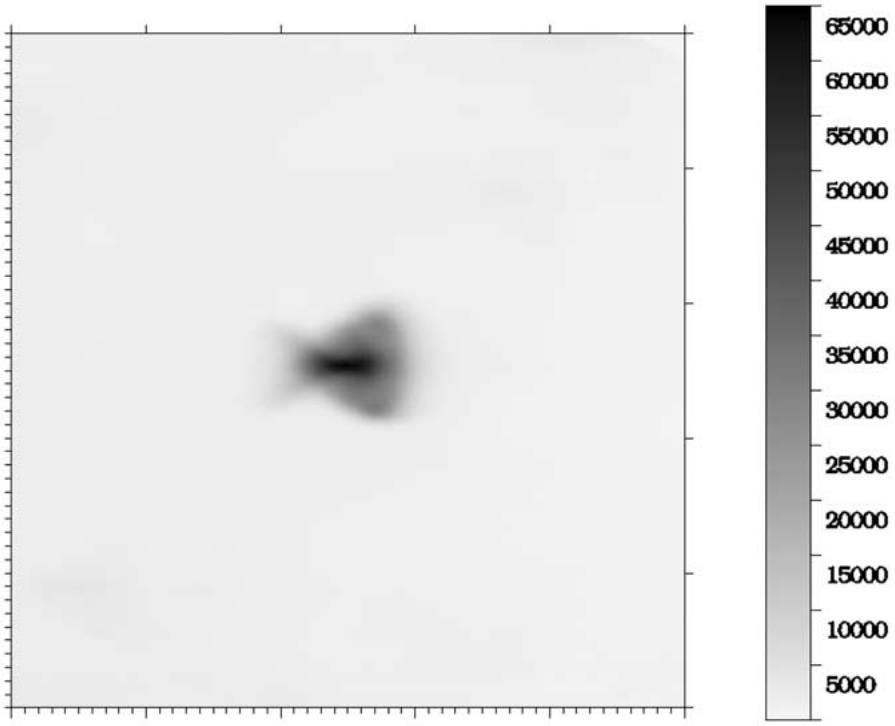


*Figure 8.* The composite image of an unresolved (point-like) object using data from the SMEI prototype optics viewing the night sky at Table Mountain, CA. This image combines approximately 100 data frames covering the transits of nine bright stars across the 3° field of view. Individual data frames for a given star are combined after transformation from CCD coordinates to a standard sky coordinate frame that is centred on the bright star's centroid. The resulting composite for each star is normalized to a peak intensity of 65 000 before averaging together to yield the above image. Major tick marks in the image correspond to roughly 1° sky angle.

### 3.2. THE MECHANICAL DESIGN

The SMEI camera shown in Figure 1 may be thought of as five pieces; these are the door, the baffle, the optics chamber, the CCD electronics box and the radiator. Each section involved inevitable design compromises in order to meet the mass, optical, radiation, thermal, and mechanical strength specifications.

#### 3.2.1. *The Door and Release Mechanism*

The door on each camera has to operate reliably only once in orbit. Until opened it is kept closed by a latch, which is released by operating a HOP designed by Starsys Research, Boulder, CO, U.S.A. The HOP has redundant heater coils. The door has a labyrinth where it interfaces with the top of the baffle rather than a seal. This design was chosen so that during launch the venting of the camera is through the door labyrinth, which provides an effective open area of around 3 $cm^2$. Upon release of the latch, strong kick-off springs open the door a few mm, when

coil springs around the hinge take over and open the door fully. A sensor indicates when the kick-off springs have started the opening sequence. The centre of the door has an aperture for mounting a calibration light emitting diode; this was removed before flight and the opening blanked off.

3.2.2. *The Baffle*

The complexity of the optical design required that the baffle be made in nine sections, of which the top section was a simple plate defining the entrance pupil. The remaining eight sections were machined from solid aluminum and sent individually to Lockheed Martin Corporation, Littleton, CO, U.S.A. for blackening. Upon completion, the baffle sections were stacked together and secured using four tensioning stainless steel tie-rods. Two of these are visible in Figure 2.

3.2.3. *The Optics Chamber*

The SMEI optics chamber contains the mirrors, the vane, and the CCD plus its mounting to the cold finger. The latter ensures that the CCD temperature is around $-35$ °C to $-30$ °C, at least for cameras which do not receive significant sunlight. In addition there is a shutter which is able to prevent light coming through the baffle from reaching the CCD. Figure 9 shows two views of the optics chamber. Figure 9(a) shows a view of the optics chamber perpendicular to the light path exiting the baffle. The shutter is circular, with two opposite quadrants removed. The shutter is controlled by a 90° stepper motor and the orientation is monitored via Hall effect sensors. The interface of the SMEI camera to the spacecraft is at the top face on Figure 9(a). The exit pupil from the baffle is visible in the form of a distorted oval.

The shutter performs two distinct functions. Firstly, if the bright object sensor, which is a simple photodiode detector located behind a black-painted mask, detects that the Sun has approached to within approximately 7° of the edge of the camera field of view then the DHU software automatically closes the shutter to avoid any risk of direct sunlight reaching the CCD. Secondly, the shutter can be closed by ground command in order to calibrate the camera. Simply closing the shutter enables the dark charge response of the CCD to be measured, whilst a flat-field calibration LED mounted on the side wall opposite the shutter provides a calibration of relative photometric response by means of light scattered off the back of the shutter. Two levels of calibration are provided by virtue of the fact that there is a white diffusing disc bonded to the back of the shutter in one of the closed positions, whilst in the other light is scattered off the black-anodized rear surface of the shutter.

Figure 9(b) shows an orthogonal view with the main optical components visible. The CCD is mounted on a solid aluminum cold finger which goes out through the side of the chamber to the passive radiator, part of which is shown schematically at the bottom of Figure 9(b). The thickness of the sides of the chamber are typically

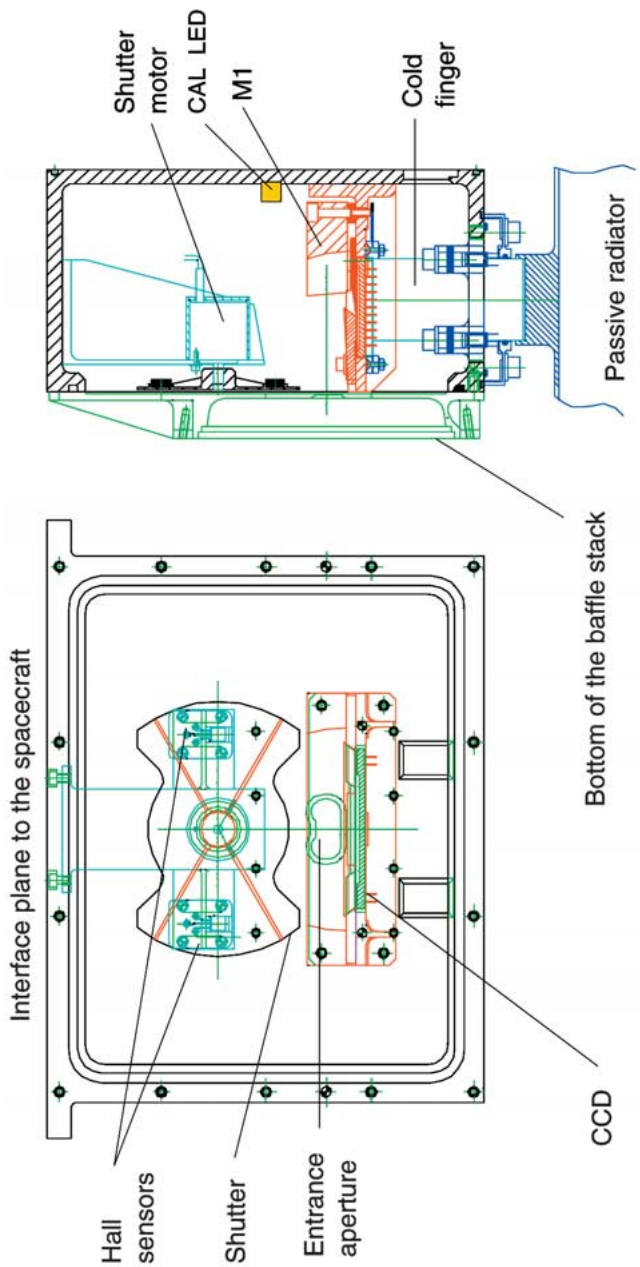


*Figure 9.* Two cross-sections of the optics chamber. (a) is orthogonal to the optical axis of the baffle, where the shutter location may be seen. The rectangular holes below the CCD are for the ribbon cables linking the CCD to its electronics box. (b) shows how the cold finger and radiator are coupled to the CCD, together with the position of the other key optical elements (*red*) shown in Figure 5.

5 mm of aluminum, which is primarily to shield the CCD from energetic electrons and ions in low Earth orbit.

#### 3.2.4. *The CCD Electronics Box and the Radiator*

The CCD electronics box primarily has to accommodate the electronics cards and power supply to operate the camera. It is designed with a wall thickness of typically 4 mm aluminum for radiation shielding.

The passive radiator is mounted onto the cold finger which passes through the top wall of the optics chamber and is also supported by two struts mounted to a bracket off the electronics box, as shown in Figures 2 and 3. The area and shape of the radiators are constrained by the overall volumetric envelope of the cameras when mounted on the spacecraft, in order to provide adequate mechanical clearances from the launch rocket fairing. SMEI has three cameras, which have different thermal environments. The Coriolis spacecraft is in a terminator orbit, such that Camera 3 is looking at the region of space closest to the Sun. Cameras 1 and 2 cover the regions of the sky from elongations approximately 120° to 180° and 60° to 120°, respectively. The area of the radiator is 480 $cm^2$ in all three cases but the radiators are rotated to different angles about an axis along the length of the cold finger to ensure that sunlight does not strike the front surface of the radiator.

Thermal isolation between the radiator and the electronics box is provided by support struts of glass-reinforced plastic (GRP). GRP is also used to provide the thermal insulation between the cold finger and the optics chamber.

### 3.3. THE CCD CAMERA

The CCD camera is based on an E2V Technologies CCD05-30-231A frame transfer device. This device employs 3-phase clocking, is front illuminated and uses Advanced Inverted Mode Operation (AIMO) technology. This technology results in a dark charge signal which is at least two orders of magnitude lower at a given temperature than that achieved using conventional technology, thereby substantially reducing the cooling requirements for the cameras. The CCD has a radiation tolerance of 10 krad. The image area has $1242 \times 576$ 22.5 $\mu$m pixels.

The sky image forms an arc on the CCD, referred to as the Region of Interest, that is selected by on-board software. SMEI operates in three basic modes: engineering mode, in which all pixels are transmitted; high-resolution mode, where there is $2 \times 2$ binning, and normal mode, where there is $4 \times 4$ binning, performed within the data handling unit. The exposure time for an image is 4 s.

The spectral response is maximum in the region around 600–750 nm, where the quantum efficiency is at least 40%. The response drops below a quantum efficiency of 10% around 450 nm in the blue side, and 950 nm on the red side. The pixel full-well capacity is $\sim 350\,000$ and the pixel-to-pixel non-uniformity is around 0.5%.

A block diagram of the CCD camera electronics is shown in Figure 10. The basic functions of the electronics are as follows:

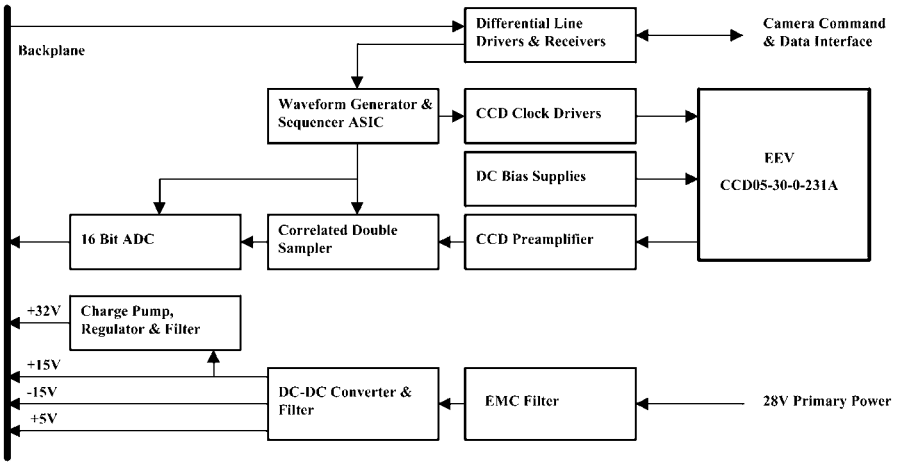


*Figure 10.* A block diagram of the CCD camera electronics.

(1) It generates waveforms and sequences of waveforms to read out the CCD in a frame transfer mode. This task is performed by an Application Specific Integrated Circuit (ASIC).

(2) It must translate the digital clocks produced by the sequencer into analogue waveforms of appropriate amplitude, voltage level and shape to drive the capacitative electrodes.

(3) It generates a number of low-noise DC bias voltages to drive the CCD's electrodes.

(4) It must amplify the video signal generated by the CCD, apply correlated double sampling (CDS) analogue processing electronics to remove CCD reset noise and reduce $1/f$ noise contributions, and finally digitize the video signal.

The video data is digitized to sixteen bits using a Crystal Semiconductors Analogue to Digital Converter (ADC). The CDS video signal processor is a balanced design to minimize susceptibility to drift, and to maximize rejection of common-mode noise.

An important aspect of the system is the power supply. This uses a space-qualified DC-DC converter from Lambda Advanced Analog, Inc, which provides a triple output at +5 V and $\pm$ 15 V. This converter employs an input emc filter and output filters to minimize switching spikes.

The programmable waveform generator and sequencer ASIC is intended for use where long, sequential waveforms are required for control and sequencing of a device such as a CCD. Sixteen bit waveforms can be produced at a frequency up to 40 MHz. The waveforms are user-programmable using a combination of sixteen bit vectors plus a table which defines the order in which the vectors are put together to define a more complex waveform. Error detection and single error correction is employed to provide some immunity to single event upsets. The ASIC

is programmed by the DHU, via an I2C serial link operating at approximately 100 kHz.

#### 3.3.1. *CCD Readout Timing*

The waveform generator ASIC uses a master clock frequency of 4.096 MHz, and 48 cycles are needed to generate the waveform required to read out each pixel. This results in a readout time of 11.72 $\mu$s pixel$^{-1}$. The exposure time for an image is 4.0 s and the previous image is read out from the CCD frame store whilst the next image is acquired. The number of active pixels in a line is 1242, plus one partially covered pixel at either end of the line; and there are an additional twenty underscan and eight overscan pixels, giving a total/line of 1272. The underscan pixels include four reference dark pixels, which are masked off from the imaged area plus sixteen dummy pixels which are available to check the noise and bias levels on the CCD. The overscan pixels are limited to four dark pixels plus four more, due to readout timing limitations. The high-speed output is differential, where an identical output transistor, but with a dummy load, is compared with the signal channel. This allows for first-order cancellation of electronic system common-mode noise such as clock feed-through and drift. One consequence of this is that it features $\sqrt{2}$ higher noise than the single channel, which results in a level of 14 electrons rms at a readout rate of around 90 kHz (11.72 $\mu$s pixel$^{-1}$). An analogue–digital unit (ADU) in the system is equivalent to around 4.7 electrons, which means that SMEI has in effect 14 bits of usable dynamic range above the noise level, and that digitization effects are not important even at the lowest signal levels. The frame transfer time is around 18 ms and the image readout time is 3.85 s. The digitized pixel data are transferred to the DHU via a high-speed synchronous link operating at 2 MHz.

### 3.4. THE DATA HANDLING ELECTRONICS

The data handling unit has the following major features:

(1) It has two fully redundant processor systems, each having interfaces to the spacecraft and the three cameras.

(2) One of the processors is in cold redundancy.

(3) There is EMI filtering and short-circuit protection of incoming spacecraft power.

(4) The DHU has DC-DC conversion and isolation for the secondary power rails.

(5) The switching of the primary spacecraft power to the cameras.

A block diagram of the DHU is shown in Figure 11. The Texas Instruments SMJ320C50AHFGM-40 processor is run with a clock frequency of 19 MHz. This is derated from the maximum possible frequency of 20 MHz. The system has a 16-bit external bus and has 9K words of on-chip RAM.

The system has a significant amount of memory. Firstly, the operating system has to be uncorruptable and this is achieved with a 128k $\times$ 8 bit E$^2$PROM (Austin

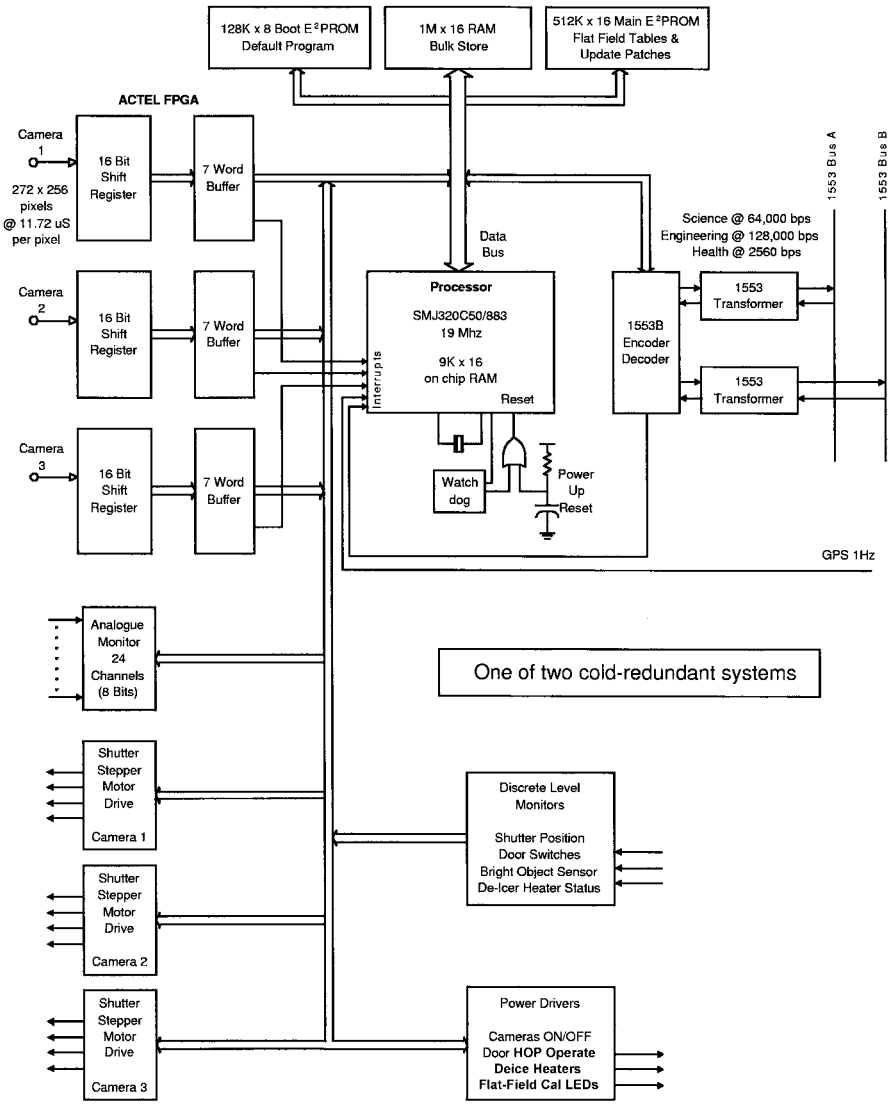


*Figure 11.* A block diagram of the DHU electronics.

AS58C1001FS-20) for boot-up code and default software. In orbit this is guaranteed write-disabled. Secondly, there is a potential need for modifications to the on-board software and corrections to the image data. A 512k $\times$ 16 bit $E^2$PROM (8 $\times$ AS58C1001FS-20) provides the memory for these tasks. The primary image correction is to apply the camera flat-field table. This was determined from calibrations prior to launch, and there is the possibility of revising the flat-field table as the data from orbital operations requires. Finally, there is 1M $\times$ 16 bit RAM (White WMS512K8-70CME) for data storage.

The main camera control is via an ACTEL Field Programmable Gate Array (FPGA) (A1460A-CQ196B) which provides the following functions:

(1) The camera interface logic, which are shift registers and 7-word input buffers.

(2) Discrete outputs for the mechanism control (see Figure 11).

(3) Discrete monitors.

(4) General glue logic (e.g., memory decoding).

The DHU has an analogue monitoring system, which includes voltages, supply currents and temperatures. Finally the interface to the spacecraft is by way of a MIL-STD-1553B transmitter-receiver (DDC BU65170S3-300). This can communicate with the redundant spacecraft interface. The whole system shown in Figure 11 is duplicated; however, only one system can be active at any one time, and the control for this is through discrete commands from the spacecraft.

Accurate timing is provided via a 1 Hz signal, coming from the spacecraft, which is derived from a GPS receiver. In the event that this signal is missing, there is a redundant system which will take over and supply an internally-generated 0.5 Hz signal until such time as the 1 Hz is restored. In the event that the 1 Hz signal is permanently lost, the SMEI internal clock can be set to provide its own 1 Hz signal; this, however, would not have the long-term stability of the GPS clock.

Finally, the DHU must be able to handle software crashes. In the event that this happens, within a short time a watchdog timer will automatically re-boot the processor. Under normal operations, the watchdog timer is reset by signals automatically generated at discrete points in the operating program.

The mass of the DHU is 6.67 kg and the normal operating power consumption is 2.9 W, going to a peak of 3.5 W. A significant amount of mass is in the housing, which was built with a typical wall thickness of 4 mm of Al to provide protection from a major fraction of the incident charged particles experienced in the Coriolis orbit. The resulting predicted dose is 1 krad year$^{-1}$. All the electronics has been designed around high reliability components, which are radiation tolerant to at least 10 krad, and protected against latch-up and single event upset.

### 3.5. THE ON-BOARD SOFTWARE

The SMEI data handling unit is a custom-built processor system designed to handle all of the in-flight functions required for operations. We now present an introduction to the on-board software and the modules used to run the instrument.

#### 3.5.1. *Architectural Overview*

The DHU is based around a Texas Instruments SMJ320C50 16-bit digital signal processor, with a MIL-STD-1553B communications bus linking it to the spacecraft. High-speed digital serial interfaces link the cameras to the DHU, and there is also provision for analogue telemetry data monitoring. The top-level hardware block diagram is shown in Figure 12.

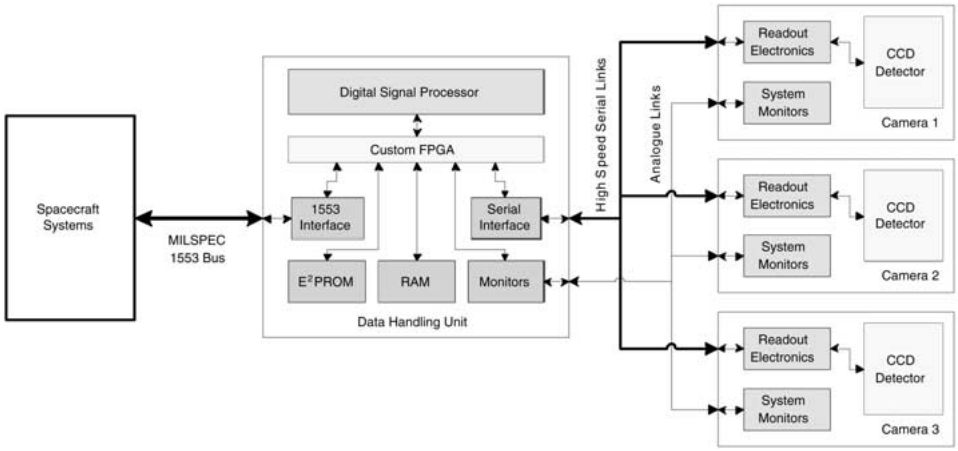


*Figure 12.* An overview of the SMEI electronics hardware.

The software controlling the DHU is written in assembler language. This was chosen primarily for performance reasons, but also to meet some interrupt service timing constraints imposed by the hardware design. Use of a high level language, such as C, would have used classes of instructions which would cause missed deadlines when servicing interrupts.

The software is written in a highly modular fashion, with each module designed with minimal dependence on other modules. A small supervisor routine cooperatively schedules the bulk of the data processing pipeline, with low-latency interrupt routines used for handling the incoming camera data stream. The overview of the software module architecture is shown in Figure 13.

### 3.5.2. *Data Processing Requirements*

The software is required to perform the following tasks to meet the science objectives.

(1) Region of Interest selection: To reduce the telemetry bandwidth requirements, the software must be able to select only the parts of the image in the active field-of-view.

(2) Flat-field correction: For accurate photometry, a gain correction factor is optionally applied to each pixel in the active field-of-view prior to binning.

(3) Pixel binning: Again, due to telemetry bandwidth requirements, the software must be able to perform data binning, with either $1 \times 1$ (un-binned), $2 \times 2$ or $4 \times 4$ bin sizes.

(4) Rice compression: To optimize the available bandwidth, a lossless compression scheme based on an algorithm presented by Rice is used. This provides compression ratios up to 2.5, depending on the image quality.

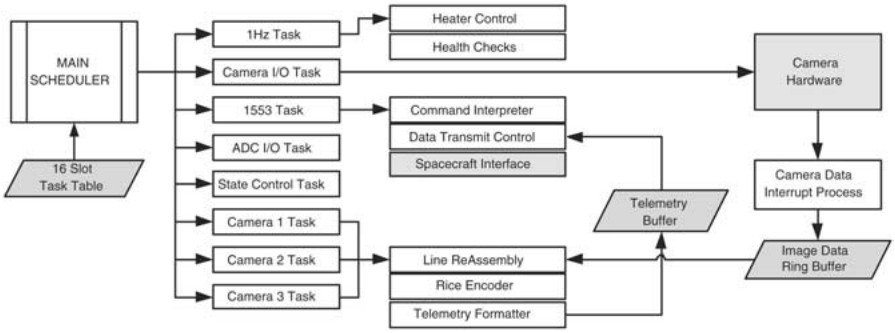


*Figure 13.* An overview of the software module architecture.

### 3.5.3. *Dataflow Interfaces*

There are three major sources of data which the DHU has to process:

(1) Camera Image Data: while gathering observational data, the cameras are producing continuous high-speed serial data of the previously-acquired image. These data are received by the DHU via a communications FIFO buffer.

(2) Spacecraft Command and Telemetry Interface: the main configuration and control of SMEI is done using the MIL-STD-1553 bus. Received commands are interpreted by the DHU, and the requisite action taken. Science data are provided to the spacecraft over this interface at either 64 000 or 128 000 bits per second. A separate 'state of health' status stream is also provided at 2560 bits per second. This contains a rotating sample of status telemetry. The DHU is able to receive and process commands at the maximum rate supported by the spacecraft bus, i.e., five commands per second.

(3) Instrument Telemetry Monitors: SMEI samples the on-board temperature, voltage, current and other monitors every second. These provide status information about the instrument and some are used as software event triggers.

### 3.5.4. *Software Modules*

As mentioned in the Introduction, the software is designed as a number of discrete and highly autonomous modules. Each module has a minimum dependence on the state of the other modules, and the system architecture is designed to be as easy to test as possible. Figure 14 shows the modules in relation to the data flow through the instrument.

(1) Camera Data Interrupt Handler: this module receives the high-speed pixel data from the camera electronics, and is responsible for pre-processing this data, and presenting it to the data handling pipeline. Incoming pixel data from each camera is routed to the FPGA on the processor card, where it is converted from serial to 16-bit wide parallel data, and stored in a seven entry deep FIFO. An interrupt is raised only after four pixels have been received in order to reduce the setup overhead of the interrupt routines, and also to relax the timing constraints on the DSP interrupt servicing latency. The routine itself performs the region of interest

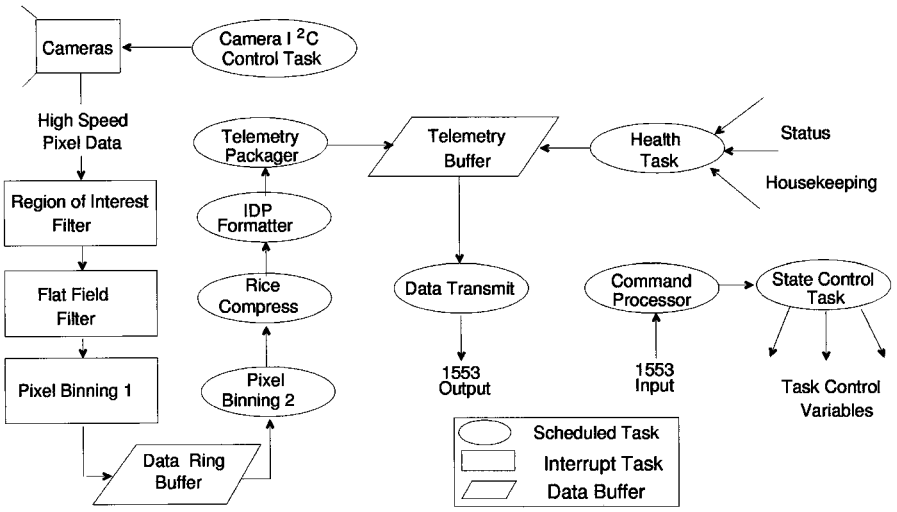


*Figure 14.* The data flow and software module relationships.

(ROI) selection process, using a pre-computed run-length encoding table designed to minimize the per-pixel processing required. If the pixels are being discarded, the routine exits. After the ROI processing, an optional flat-field correction is applied to each pixel. This is a simple 32-bit multiplication, with the top 16 bits of the result being taken for further processing. After the flat-field correction, the pixels are binned to $1 \times 1$, $2 \times 1$ or $4 \times 1$, and a 32-bit result is written to the large per-camera ring buffers. A pre-scaling factor is also applied to ensure that the 16 most significant bits of the resulting bin appear at the same offset after binning is completed, reducing processing slightly.

(2) Inter-Line Binning and Rice Compression: this routine processes data from the interrupt-routine filled ring buffer into line binning buffers. A pre-computed table is used to identify the end of each line, and once the samples from the ring buffer have been accumulated over 1, 2, or 4 lines depending on the bin mode, the line assembly buffer is flagged as completed. The most significant 16 bits of the bin are taken. Thus the 4 least significant bits of the sum are discarded in $4 \times 4$ binning mode, and 2 bits in $2 \times 2$ binning mode.

Completed and optionally binned lines are then optionally Rice-compressed. The compression algorithm splits each bin value along the line into two parts - a set of least significant bits, which are assumed to be random noise and a signal component from the remaining most significant bits. The noise bits are telemetered, whilst the differences in signal components between successive bins are efficiently encoded. This achieves a compression ratio of 2.5 with most camera data, though it degrades to 0.8 during charged particle enhancements seen during parts of the orbit.

(3) Error Correction and Telemetry Formatting: the next stage of data processing after the Rice compression is the encoding of the resulting bit stream into a format

suitable for transmission to the spacecraft solid state recorder, and ultimately to the ground. The design criteria for this were that we should not lose more than 0.1% of the data due to the bit error rate on the down-link path. To meet these criteria, and to keep the processing power requirements to a minimum, a simple error correction scheme based on parity calculations is used. The image data is split into blocks of 256 16-bit words, arranged as a 4 column by 64 row array. Parity is calculated for each row and column, and the resulting 8 16-bit words of parity are added to the block of image data, to create an image data packet (IDP) of 264 16-bit words. These IDPs are loaded into the camera telemetry buffers, ready for multiplexing by the transmission control module. Depending on the camera operating modes (i.e., on-board binning mode and the number of cameras operating), and also the science data rate to the spacecraft (i.e., 64 000 or 128 000 bits $s^{-1}$) there may not be enough space in the telemetry buffer for the whole image, in which case the frame is discarded, and one of two strategies is followed for resuming image frame storage for the camera that filled the output telemetry buffer.

The first strategy is aimed at creating continuous blocks of consecutive frames, and after the overflow, frames are only stored again once the telemetry buffer is completely emptied. This gives the maximum amount of buffer space for contiguous frames, but can lead to long periods of time between frames, and gaps in the sky coverage.

The second strategy is a trickle-feed strategy, which aims to ensure that there are no missing areas in the sky fields. In this mode, the processor continues to attempt to queue up successive frames, and so maintains the minimum inter-frame time gap, and a mostly full telemetry buffer. In both cases, the average number of frames stored over a long period of time is the same; Figure 15 compares the overall number of frames stored as a function of time, with a single camera operating with no on-board binning.

(4) Camera Configuration and Control: each of the three cameras has a set of camera control electronics, and the CCD waveform generation ASIC is controlled by the DHU using an I2C link. The waveforms are loaded, and frame readouts started by issuing transactions over this link. The hardware in the DHU for controlling this link is a simple 2-bit register controlling the clock and data lines of the link. This module is responsible for enforcing the I2C state machine on each link, and for providing link contention arbitration during camera initialization, and observing modes. The link is run at around 100 kHz, though the exact speed depends on the current processor loading in the DHU.

(5) Shutter Stepper Motor Control: each camera has a 4-phase stepper motor, with a shutter having two closed and two open positions. This module maintains a unified motor command queue for the three cameras to enforce a power budget limit, namely that only one phase of the shutter motors can be powered at one time. Commands in the queue identify the camera, the phase to power, and the duration of the power and dwell times. This module provides mechanisms to flush the queue in an emergency condition, and to rapidly close all the shutters.

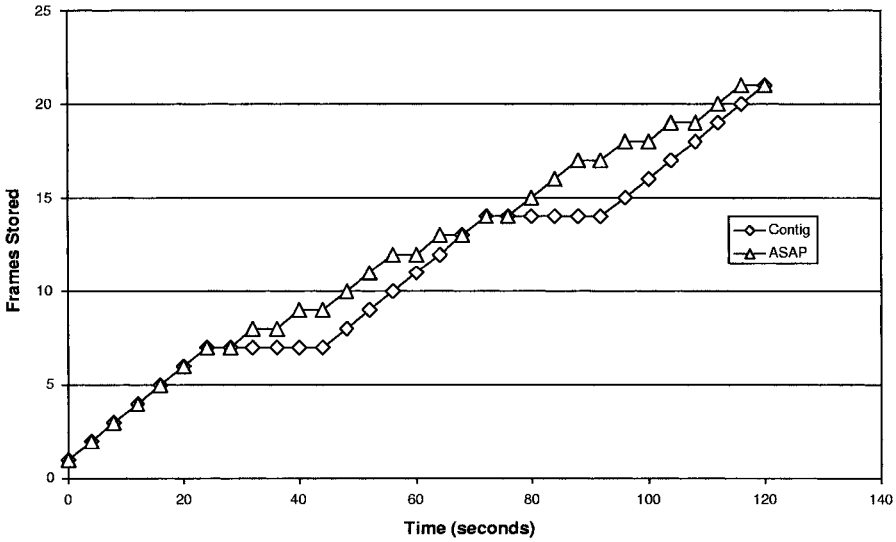


*Figure 15.* Frame storage comparisons with no on-board binning. The lower plot (*diamonds*) shows the number of frames stored as a function of time if continuous blocks of data are stored. The upper plot (*triangles*) shows the same, but using the trickle-feed strategy (see text).

(6) Thermal Control and Stabilization: the CCD in each camera is mounted on a cold-finger and attached to a radiator, to maintain the CCD at a cool temperature for better CCD performance. This module provides functions to control a heater attached to the cold finger. The temperature of the CCD can be stabilized around the orbit to approximately $\pm 1$ deg. The temperature can also be set to maintain the CCD at a temperature much warmer than the surrounding enclosure. This mode was used to prevent contamination during early orbit operations, ensuring that any contaminants were preferentially deposited on the colder surroundings, and not the sensitive detector.

(7) 1553 Communications and Command Interpreting: this module is responsible for managing access to the intelligent hybrid device used for interfacing to the spacecraft MIL-STD-1553B bus. It arbitrates access to the on-hybrid buffers, ensuring that the transmission buffers are always kept up to date, and received commands and data are loaded into the appropriate queues for other modules. This module also contains the command interpreter, which processes mode transition and configuration requests.

(8) Telemetry Acquisition and Event Triggers: this module is responsible for reading and updating the analogue and digital monitors for the instrument. It also sets the flags used during bright object transitions through the field of view. If a camera bright object sensor reads 'bright' for 5 s, the shutter is closed until the sensor returns to normal.

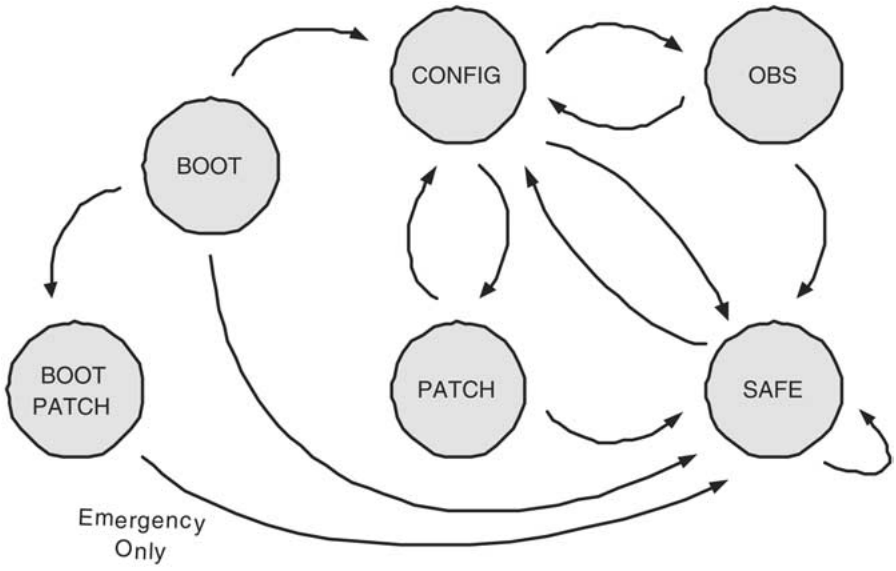


*Figure 16.* Permitted mode transitions.

3.5.5. *Instrument Operating Modes*

The instrument has a number of operating modes, and Figure 16 shows the permitted state transitions.

Each major operating mode has a subset of the total commanding available. This greatly reduces the complexity of the inter-module locking by removing many possible interactions. Most commands are only available in configuration mode, and so almost all of the software modules are quiescent and changing controlling parameters is a straightforward matter.

(1) Boot Mode: this is the mode in which the instrument starts after power-up. The DHU has 8 identical copies of the at-launch software image in a non-volatile, write-protected store, and while in this mode one of these copies is running. The multiple copies provide redundancy in the case of a bit error developing in one of the copies. The capability also exists to upload a new software image to a dedicated area of non-volatile store. If a patch is present, entering configuration mode loads the new patch, and starts it running. This two-step boot process allows recovery from a corrupted upload.

(2) Configuration Mode: this is the main mode for changing thermal stabilization, camera observing modes and overall system parameters. SMEI will normally have the cameras switched on, but is not acquiring frames in this mode. Transition to observing mode causes the camera waveform generators to be reinitialized, the shutter queue to be loaded for the configured observation, and frame capture to begin.

(3) Patch Mode: this mode is used to update the on-board non-volatile store. The store contains flat-field tables, observation default settings, command interpreter

tables and other critical data. This mode is also used for uploading a new software image.

(4) Safe Mode: this mode is used when a spacecraft emergency command is received. SMEI immediately switches off all non-essential power, and performs a rapid shutter close sequence. Thirty seconds later the spacecraft switches off power to the instrument entirely.

(5) Observing Mode: this is the primary mode for the instrument. The selected observation configurations are enabled, and the shutters are repositioned to the desired positions. Frames are requested from the cameras at 4-s intervals, and the data processing outlined in Section 3.5.2 is executed.

#### 3.5.6. *Instrument Observing Configurations*

The baseline operating mode of the instrument for scientific observations was to acquire images from all three cameras every 4 seconds with on-board binning of $4 \times 4$ pixels. In this configuration all image data, together with associated housekeeping and state-of-health data, could be down-linked via the spacecraft MIL-STD-1553B bus at a data rate of 64 000 bits per second.

An alternative science observing configuration, which became the normal operating mode, is to operate two cameras with $4 \times 4$ pixel binning and the third camera with $2 \times 2$ pixel binning. This requires the spacecraft bus to collect data at 128 000 bits per second to avoid loss of images and there are stricter limitations on the period over which the spacecraft solid state recorder can acquire SMEI data between data down links.

Calibration and engineering data (e.g., dark charge and flat-field calibration images) are generally acquired without on-board pixel binning. Due to data rate and on-board software table allocation issues, only one camera may be operated at a time in this configuration.

### 3.6. The Spacecraft Interface

The electrical interface was discussed in Section 3.4. The mechanical interface to the spacecraft is complex. The payload must be mounted such that each camera covers a different $60^\circ \times 3^\circ$ area of the sky in the zenith-facing hemisphere. Furthermore, the cameras must be mounted such that the unwanted brightness entering each baffle from any or all of the spacecraft or payload appendages does not exceed the design limits on stray light necessary to achieve the performance indicated in Figure 1.

The approximate look directions of the three cameras are given in Table I. It is important to mount the cameras such that they see as much as possible of the dark sky, and without camera 3 seeing the Sun. To achieve this in the terminator orbit, camera 3 was mounted so that typically the closest edge of the field of view is around $20^\circ$ away from the Sun. The precise angle varies over a range from $-16^\circ$ to $32^\circ$ depending on the position of the spacecraft in its orbit and the season.

TABLE I
The Euler angles for the three cameras.

| Camera number | Look direction | $\phi$ | $\theta$ | $\psi$ |
|---|---|---|---|---|
| 1 | Anti-Sun | −28 | +70 | −22 |
| 2 | 90° from Sun | −86 | +58 | −7 |
| 3 | Sunward | −144 | +62 | 0 |

As shown in Figure 3, each camera has coordinate axes $X_c$, $Y_c$, $Z_c$ and they need to be rotated from the spacecraft coordinate axes $X_{sc}$, $Y_{sc}$, $Z_{sc}$ using Euler angles. Here $+Z_{sc}$ is defined as the zenith direction, $+X_{sc}$ is the spacecraft velocity direction and $Y_{sc}$ is approximately sunward. Table I shows the Euler angles which give the pointing directions for the three cameras.

The first angle, $\phi$, describes a rotation about the $+Z_{sc}$ axis to define a new $+X_c$ axis about which the second rotation, $\theta$, will take place. After these rotations, the new $Z_c$ axis defines the baffle centre line. The final angle, $\psi$, defines the amount of rotation of the baffle's long dimension, about the $+Z_c$ axis.

The mounting of each camera must allow sufficient room for its door to open, and when open, stray light from the door must not enter the field-of-view of either of the remaining cameras. Finally, the mounting must be such that the passive radiator on the cold finger attached to each CCD should have a sufficient view angle to deep space to meet the cooling requirements for the CCD.

### 3.7. THE THERMAL DESIGN

The cameras are mounted on struts so that they are thermally isolated from the spacecraft structure. Cameras 1 and 2, whose baffle apertures are mainly exposed to deep space, have their outer surfaces covered with Multi-Layer Insulation (MLI). Camera 3 has around 40 W of solar input into the baffle, so the problem here is to keep the baffle as cold as possible. Thus the majority of the outer surfaces of this camera are covered with high-emissivity radiator tape, rather than MLI. The angles of the passive radiators to the camera axes were computed to prevent sunlight from striking the front faces of the radiators. The backs of all radiators were covered with MLI, whilst the front surfaces were covered with high-emissivity tape.

The design goal for the cameras is to allow the CCD chip to reach a temperature of around −30 °C. Stabilization of the temperature is by means of heaters. Following spacecraft integration and the resulting final thermal balance test, the effect of the radiators on these cameras was trimmed by fitting MLI over different fractions of the radiator surface, to give a CCD temperature in the required range. It was later discovered that it was not possible to achieve a CCD temperature of −30 °C for camera 3; its operating temperature is typically around −6 °C. This higher

than optimal temperature results from a more difficult thermal environment for this camera than the others. A cooler operating temperature for camera 3 was not feasible within the timing of the Coriolis payload delivery schedule, and technology transfer restrictions.

## 4. Instrument Calibration and Qualification

The instrument was calibrated optically and environmentally tested to ensure survival on launch, and freedom from undesirable electromagnetic effects.

### 4.1. Optical calibration

The optical tests were in two parts. The first test was to verify the performance of the baffle. The tests consisted of measuring the light coming through the final aperture Z0 (Figure 4) as a laser beam illuminated a variety of spot locations within the baffle. The light was measured using a CCD camera which viewed Z0 through a wide-angle lens. The results showed that the baffles achieved a fractional reduction in light intensity ranging from $0.8 \times 10^{-10}$ to $1.3 \times 10^{-10}$ for the three flight baffles and the spare unit. The specification was for a reduction of $10^{-10}$.

The second consideration is the photometric test. A fundamental performance specification for SMEI is that each camera deliver 0.1% differential photometric precision as stars and other objects move across the CCD. The next stage is to handle the inevitable sub-pixel response gradients which we have measured at typically a few percent. Our design controls these variations by defocusing the image, so that point sources, such as stars, are spread over many pixels. This provides a robust optical design, which averages over the sub-pixel variations and enables us to reach our photometric goal.

The method we used to calibrate each set of optics, together with their individual CCD chips, is as follows. A light source was constructed using 0.5 mm diameter fiber optics which delivered the light from a single halogen bulb, powered by a regulated power supply, to a line of spots placed on the surface of a cylinder of radius 1 m, and spaced 3° apart as viewed from the cylinder axis. Each camera under test was placed with aperture Z0 as close as possible to the cylinder axis so as to view the array of spots. The CCDs were shimmed by around 0.75 mm further from M2, to focus on the sources. Following an exposure, the light sources were then moved by a known amount, and another exposure taken. The discrete translation steps for the light source were equivalent to about 0.1 CCD pixels, and spanned about five pixels. Checks were made on the stability of the source, whose spots were found to maintain the same relative brightness to within a tenth of a percent over several hours.

Following the calibrations, the flight systems were verified to pass the 0.1% photometry requirement, by confirming the stability of the relative photometric brightness of the spots as the array moved over the pixels.

### 4.2. TESTING AND QUALIFICATION

The engineering model was vibrated to a random input level of 19.3 g (r.m.s.) in the $X$ and $Z$ axes, and to 9.7 g (r.m.s.) in the $Y$ axis. When this qualification test was made (August, 1999) it was unclear what the spacecraft and launch vehicle were going to be; consequently SMEI was tested to the levels employed for the DMSP spacecraft. A full level sine vibration was performed over the frequency range 5–100 Hz. The instrument suffered no damage during these tests.

Some other noteworthy items are as follows:

– A low level resonance search was performed and there were no significant resonances below 76 Hz.

– The instrument conforms to US Military specification MIL-STD-461D for electromagnetic compatibility.

– The assembly and testing of the flight instrument were conducted in a Class 1000 clean room.

## 5. Summary

We have described a novel instrument which is operating successfully in orbit. The primary objective is to observe coronal mass ejections and other heliospheric structures and forecast their Earth arrival. If the primary SMEI objective is met at the design resolution of 1 deg, then we will know the light curves for over 40 000 locations in the sky to an accuracy better than 0.1% down to the 10th magnitude level. This will enable SMEI to monitor zodiacal cloud transient phenomena, comets, and variable stars over the whole sky with unprecedented accuracy. Comet NEAT (2002 V1) was observed in February 2003, and exemplifies the many serendipitous brightness changes that doubtless can be monitored by this instrument.

The secondary objective is to be able to provide light curves to the design photometric accuracy, or better, of interesting sky objects. In principle this could apply to most of the 200 000 stars above around 10th magnitude. This will enable SMEI to monitor variable stars, bright supernovae, near-Earth objects and comets. Comet NEAT was observed in February 2003. In addition, we have every expectation that the data will be useful in searching for extra-solar planets, especially those of Jovian size in close orbit around their parent star.

## Acknowledgements

SMEI has been built at the University of Birmingham under Contract F19628-96-K-0005. Funding for SMEI has come from the USAF, NASA and the University of Birmingham. Mr M. J. Deeley made a significant contribution to engineering the production of the SMEI hardware from the conceptual drawings. The initial electronics design was made by the late Mr P. M. Thompson; the design was

completed with assistance from Mr D. Hoyland. Dr S. M. Mahmoud and Ms H. Mapson-Menard contributed to the theoretical mechanical and thermal designs. Ms R. Sagalyn gave valuable encouragement at the beginning of the programme. We acknowledge the support given by Dr S. Keil and Dr R. R. Radick, who have successively acted as Principal Investigator for SMEI. Dr R. E. Gold contributed an earlier design concept for SMEI. The support of Ms J. C. Johnston, SMEI Programme Manager, is gratefully acknowledged. We thank Drs R. R. Radick and D. F. Webb for constructive comments on the manuscript.

## References

Buffington, A., Hudson, H. S., and Booth, C. W.: 1990, *Publ. Astron. Soc. Pacific* **102**, 688.
Buffington, A., Booth, C. W., and Hudson, H. S.: 1991, *Publ. Astron. Soc. Pacific* **103**, 685.
Buffington, A., Jackson, B. V., and Hick, P. P..: 2002, *SPIE Proc.* **4853**, 490.
Jackson, B. V. and Hick, P. P.: 2002, *Solar Phys.* **211**, 345.
Jackson, B. V. and Leinert, C.: 1985, *J. Geophys. Res.* **90**, 10759.
Jackson, B. V. *et al.*: 2003, *Solar Phys.*, submitted.
Leinert, C., Pitz, E., Link, H., and Salm, N.: 1981, *Space Sci. Instrum.* **5**, 257.
Martin Marietta Company: 1977, *SPIE Proc.* **107**, 168.